Electronic Supplementary Material (ESI) for Energy & Environmental Science.
This journal is © The Royal Society of Chemistry 2024

Supporting Information

The deconstruction of polymeric solvation cage: a critical promotion strategy on PEO-based all solid polymer electrolytes

Ruiyang Li[a], Haiming Hua[a], Xueying Yang[c], Jianling Tian[c], Qichen Chen[c], Rongwei Huang[d], Xue Li[d], Peng Zhang[c*], Jinbao Zhao[ab*]

[a]College of Chemistry and Chemical Engineering, State-Province Joint Engineering Laboratory of Power Source Technology for New Energy Vehicle, State Key Laboratory of Physical Chemistry of Solid Surfaces, Engineering Research Center of Electrochemical Technology, Ministry of Education, Collaborative Innovation Center of Chemistry for Energy Materials, Xiamen University, Xiamen, 361005, PR China

[b]Innovation Laboratory for Sciences and Technologies of Energy Materials of Fujian Province (lKKEM), Xiamen 361005, China

[c]College of Energy, Xiamen University, Xiamen 361102, Fujian, China

[d]National Local Joint Engineering Research Center for Lithium-ion Batteries and Materials Preparation Technology, Key Laboratory of Advanced Batteries Materials of Yunnan Province, Faculty of Metallurgical and Energy Engineering, Kunming University of Science and Technology, Kunming 650093, PR China

*Corresponding authors.

E-mail addresses: jbzhao@xmu.edu.cn (J. Zhao), pengzhang@xmu.edu.cn (P. Zhang)

Experimental

Materials characterization

The differential scanning calorimetry (DSC) curves were conducted on a Model STA 449 instrument (NETZSCH Machinery and Instruments Co., Ltd.) to investigate the enthalpy change of the SPE with a heating rate of 10 K/min. To investigate the interactions between different species in the SPE, the attenuated total reflection infrared (ATR-FTIR) spectroscopy was tested with a Nicolet IS5 spectrometer in the range of 600–4000 cm^{-1}. ^{7}Li nuclear magnetic resonance (NMR) spectra conducted on Bruker 500 MHz at room temperature, among which, PEG (*Mv*=1000, Aladdin) is used as the model of PEO due to its liquid state at room temperature after the addition of LiTFSI. The reference consisted of 0.1 M $LiClO_4$ dissolved in D_2O in a sealed capillary tube. The capillary tube was coaxially inserted into the NMR tube filled with the electrolyte sample. Raman spectroscopy (Horiba LabRAM HR Evolution) was used to characterize the interaction in SPEs with a 532 nm wavelength of laser.

The crystalline calculation equation is as follows:

$$X_c = \frac{\Delta H_f}{\Delta H} \times \frac{1}{w_f} \times 100\%$$

In this equation, X_c is the crystallinity of SPE membrane, ΔH_f is the integral value of melting enthalpy, ΔH is the melting enthalpy of 100% crystallized PEO which value at 213.7 J/g, and w_f is the weight ratio of PEO.

The electrochemical impedance spectroscopy (EIS) on an electrochemical Solartron workstation at a frequency range from 0.1 to 10^5 Hz with a voltage amplitude of 10 mV to measure the σ of SPE membrane. The σ at different temperatures was obtained by the following formula:

$$\sigma = l/(R \times A)$$

In this formula, σ is the ionic conductivity of SPE membrane, l refers to the thickness of SPE membrane, R is the resistance of the electrolyte membrane and A is the area of the stainless steel (SS). In addition, PEG is used as the model of PEO to investigate the effect of chain entanglement on σ, the *Mv* range is set at 300, 1000, 4000, 10000, 20000 g/mol (the number of repeating EO units range from 6 to 450). By potentiostatic polarization method on an Autolab electrochemical

workstation (Metrohm, Switzerland) with a Li|SPE|Li simulating cell, the t_{Li+} was calculated by the equation:

$$t_{Li+} = \frac{I_{SS}(\Delta V - I_0 R_0)}{I_0(\Delta V - I_{SS} R_{SS})}$$

In this equation, ΔV was set at 10~20 mV, I_0 and R_0 represent the initial current and interfacial resistance, I_{SS} and R_{SS} were the final ones. (To ensure the accuracy of the test, the PEO-40-10 (SPE1100) with TTE is fully polarized, hence, 10 mV for PEO(600k)-40-10 with TTE, PEO-12 with TTE, PEO-10 with TTE and PEO-40-10 (SPE2900) with TTE; 20 mV for PEO-40-10 (SPE1100) with TTE)

Molecular dynamics simulation

The molecular dynamics simulations (MD) were performed via GROMACS 2018.8[1] software. For the visualization of simulation boxes, the VMD[2] software was used. We employed the OPLS-AA[3] force field and the force field parameters of each molecule were taken from the previous works[4-6], which is suitable for describing the SPE systems. In order to correct the polarization effect among anions and cations[7, 8], atomic charges of ions were multiplied by a scale factor of 0.78. The models of PEO and TTE are shown in the Figure S4, containing 22 polymer chains and 55 LiTFSI in the electrolyte boxes generated by Packmol software. Firstly, boxes were submitted to energy minimization via the steepest-descent method and the equilibrium simulation was carried out under the NPT ensemble at 1 bar. Secondly, an annealing method was used to obtain an equilibrium system, the system ran at 598.15 K for 20 ns, and then cooled to 353.15 K within 40 ns, then ran at 353.15 K for 20 ns. Finally, the production simulation ran for 10 ns at 353.15 K with a time step of 2 fs and a verlet algorithm. An Ewald summation routine was used for long-range forces (rcut = 10 Å), and the data were collected every 20 ps. The σ was performed via an NVT ensemble with an electric field of 0.1 V/nm[7, 9]. The σ and t_{Li+} were calculated by formula (1) and (2), respectively, in which v is average drift rate, c is ion concentration, E is electric field strength, Z is the valence state of ion, and F is Faraday constant. The radial distribution function (RDF) was analysed by Gromacs.

$$\sigma = \frac{v^+}{E} \cdot c^+ \cdot |Z^+| \cdot F - \frac{v^-}{E} \cdot c^- \cdot |Z^-| \cdot F. \quad [1]$$

$$t_{Li+} = v^+ \cdot |Z^+| / (v^+ \cdot |Z^+| - v^- \cdot |Z^-|). \quad [2]$$

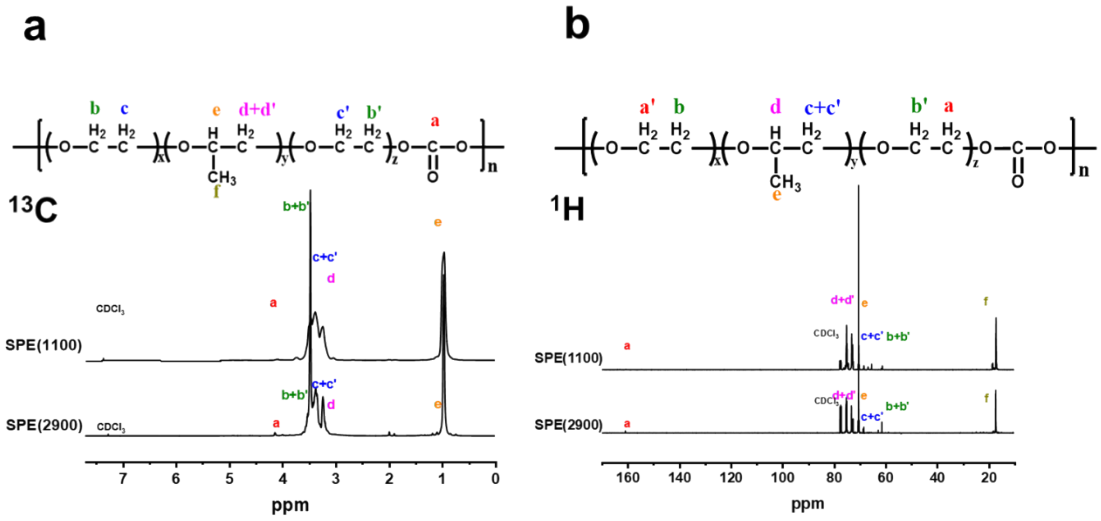

Figure S1 (a) ^{13}C and (b) ^{1}H NMR of SPE1100 and SPE2900

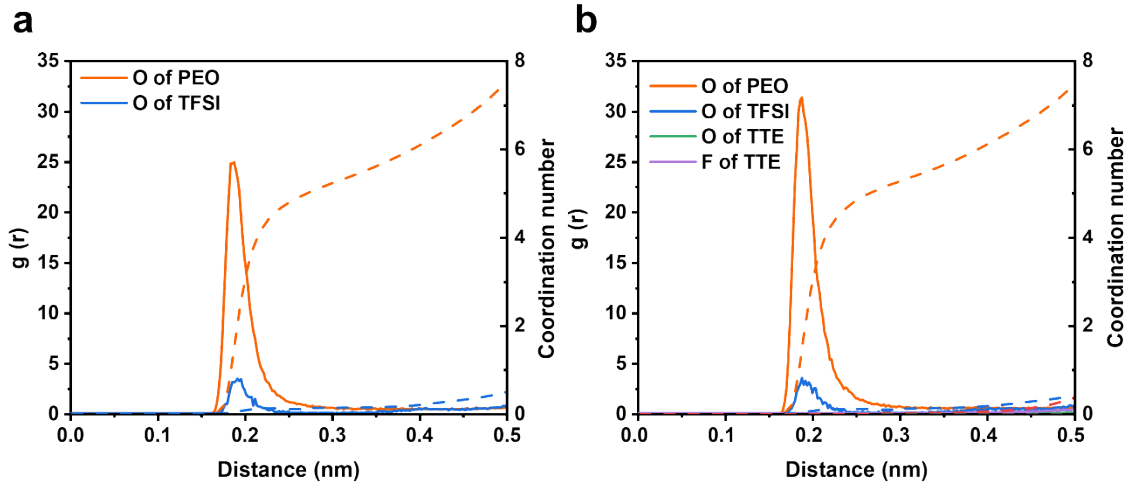

Figure S2 RDF of PEO_{20}LiTFSI and PEO_{20}LiTFSI with TTE

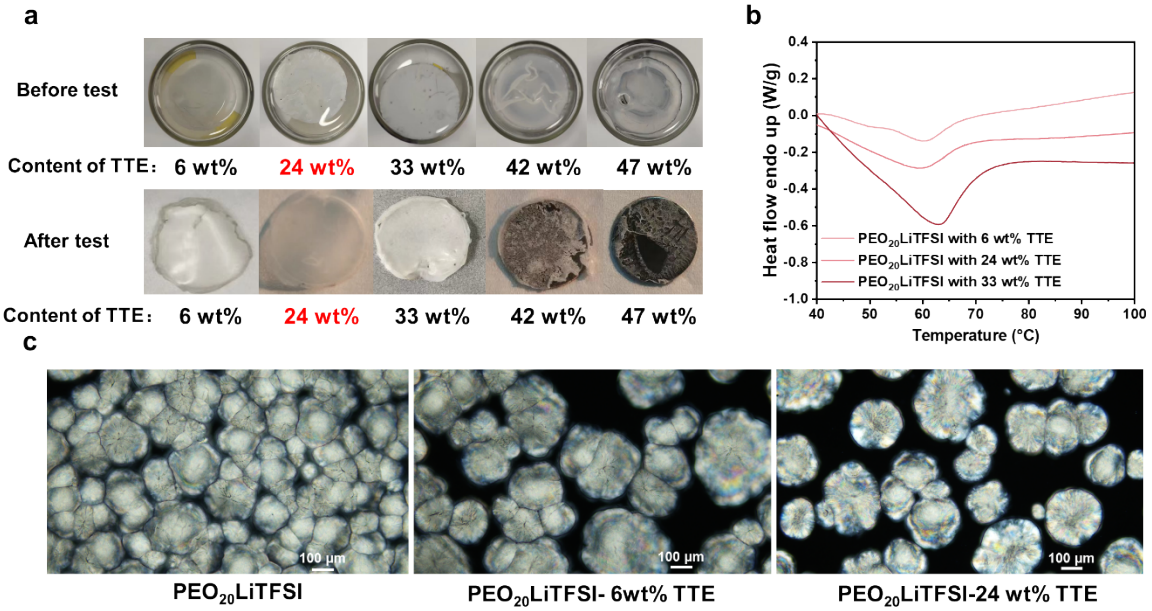

Figure S3 (a) The optical microscope images of PEO_{20}LiTFSI film with different TTE content before and after Arrhenius plots test;(b) DSC traces of PEO_{20}LiTFSI film with different TTE content; (c) The optical microscope images of PEO_{20}LiTFSI with 24wt% TTE

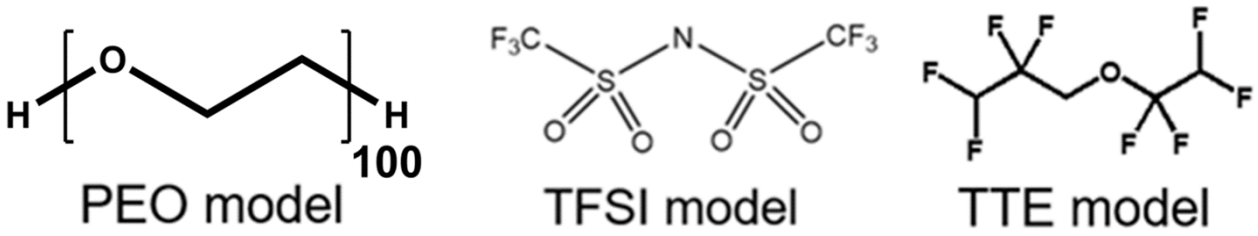

Figure S4 Molecules used in MD simulations

Table S1 The ionic conductivity of PEO-20 and PEO-20 with TTE from MD simulation at 80 ℃

	$PEO_{20}LiTFSI$	$PEO_{20}LiTFSI$ with TTE
δ (Li^+) (S/cm)	2.2×10^{-4}	7.0×10^{-4}
δ (total) (S/cm)	4.4×10^{-4}	1.41×10^{-3}

Table S2 The ionic conductivity of PEO(600k)-20 and PEO(600k)-20 with TTE at 25 ℃

	δ (S/cm)
PEO(600k)-20	5.7×10^{-6}
PEO(600k)-20 with TTE	2.6×10^{-4}

Table S3 The crystallinity of $PEO_{20}LiTFSI$ with different weight ratio of TTE

	Crystallinity (%)
$PEO_{20}LiTFSI$	49.9
$PEO_{20}LiTFSI$ with 6 wt%TTE	25.6
$PEO_{20}LiTFSI$with 24 wt%TTE	19.5
$PEO_{20}LiTFSI$ with 33 wt%TTE	10.7
PEO (Mv=600k)	65.0
PEO (Mv=100k)	42.8
PEO-40-10 with TTE (Mv=600k)	10.7
PEO-40-10 with TTE (Mv=100k)	0.0

Table S4 The crystallinity and σ of $PEG_{20}LiTFSI$ with different *Mv*

	PEG1000 n(EO)~23	PEG4000 n(EO)~91	PEG10000 n(EO)~227	PEG20000 n(EO)~454
Crystallinity (%)	3.4%	4.3%	36.0%	39.8
$\delta \times 10^{-5}$ (S/cm)	2.3	1.81	0.0369	0.0544

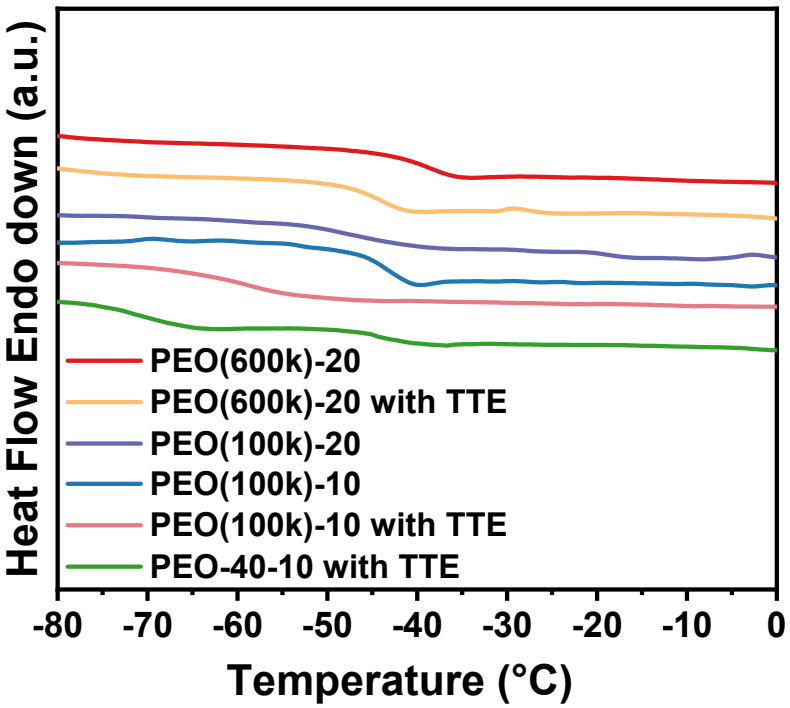

Figure S5 (a) DSC traces of PEO(600k)-20, PEO(600k)-20 with TTE, PEO(100k)-20, PEO(100k)-10, PEO(100k)-10 with TTE and PEO(100k)-40-10 with TTE(SPE1100)

Table S5 The Tg of PEO(600k)-20, PEO(600k)-20 with TTE, PEO(100k)-20, PEO(100k)-10, PEO(100k)-10 with TTE and PEO-40-10 with TTE(SPE1100)

	Tg (°C)
PEO(600k)-20	-40.1
PEO(600k)-20 with TTE	-45.6
PEO(100k)-20	-46.2
PEO(100k)-10	-42.8
PEO(100k)-10 with TTE	-59.3
PEO-40-10 with TTE(SPE1100)	-69.6

Table S6 The σ, t_{Li+} and σ_{Li+} of PEO-12 with TTE, PEO-10 with TTE, PEO-40-10 (SPE2900) with TTE and PEO-40-10 (SPE1100) with TTE at 25 ℃

	δ (S/cm)	t_{Li+}	δ_{Li+} (S/cm)
PEO-12 with TTE	2.6×10^{-4}	0.28	7.3×10^{-5}
PEO-10 with TTE	1.3×10^{-4}	0.22	2.9×10^{-5}
PEO-40-10 (SPE2900) with TTE	2.4×10^{-4}	0.46	1.1×10^{-4}
PEO-40-10 (SPE1100) with TTE	3.2×10^{-4}	0.57	1.9×10^{-4}

Table S7 The activation energy and coefficient of determination (R^2) of PEO-40-10 with TTE, PEO-10 with TTE and PEO-10

	PEO-40-10 with TTE	PEO-10 with TTE	PEO-10
Ea (kJ/mol)	14.39	16.07	41.10
R^2	0.994	0.995	0.994

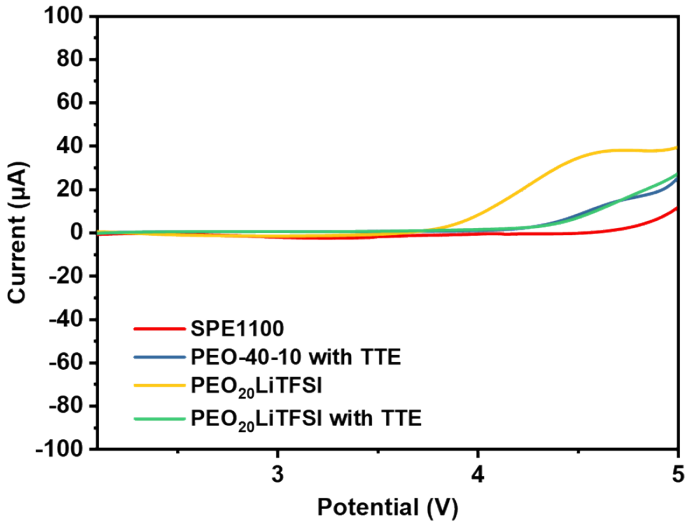

Figure S6 The electrochemical stability window of PEO_{20}LiTFSI, PEO_{20}LiTFSI with TTE, SPE1100-10 and PEO-40-10 with TTE.

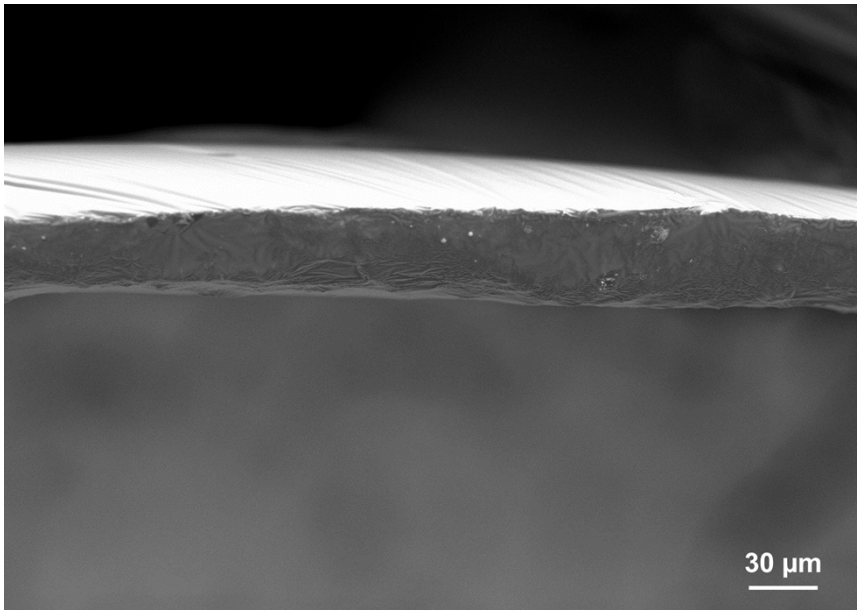

Figure S7 The SEM of PEO-40-10.

Table S8 The ionic conductivity and Li^+ transference number of traditional plasticizers for PEO-based systems comparing with this work

	Addition	Ionic conductivity (RT)	Li^+ transference number
In this work	PEO+TTE+SPE1100	3.2×10^{-4} (25 ℃)	0.57
7	PEO+Al_2O_3	$<10^{-5}$ (RT)	0.48
8	PEO+EC+PC	1.2×10^{-4} (RT)	-
9	PEO+$Li_{10}GeP_2S_{12}$ +SN	9.1×10^{-5} (25 ℃)	0.20
10	PEO+LLZTO+SN	1.22×10^{-4} (30 ℃)	0.41
11	PEO+DME	1.03×10^{-3} (30 ℃)	0.51
12	PEO+LLZO	1.2×10^{-4} (25 ℃)	0.41
13	PEO+1,4-DITFB	1.2×10^{-4} (25 ℃)	0.35
14	PEO+CeF_3	3.08×10^{-5} (30 ℃)	0.35
15	PEO+CuF_2	2×10^{-4} (30 ℃)	0.42
16	PEO+LiI	2.1×10^{-4} (45 ℃)	0.32

Table S9 The full width at half maximum (FWHM) of PEO_xLiTFSI with TTE and PEO_xLiTFSI without TTE in FTIR (Mv=600k)

	The FWHM of peak located at 1100 cm^{-1} (cm^{-1})	The FWHM of peak located at 844 cm^{-1} (cm^{-1})
PEO_6LiTFSI	14.7	24.4
PEO_6LiTFSI with TTE	19.9	32.1
PEO_{12}LiTFSI	15.0	25.1
PEO_{12}LiTFSI with TTE	20.3	33.5
PEO_{20}LiTFSI	14.7	25.4
PEO_{20}LiTFSI with TTE	20.6	34.8

Table S10 The full width at half maximum (FWHM) of $PEO_xLiTFSI$ with TTE and $PEO_xLiTFSI$ without TTE in Raman (Mv=600k)

	The FWHM of peak located at 280 cm^{-1} (cm^{-1})
$PEO_6LiTFSI$	6.2
$PEO_6LiTFSI$ with TTE	6.7
$PEO_{12}LiTFSI$	6.2
$PEO_{12}LiTFSI$ with TTE	7.3
$PEO_{20}LiTFSI$	6.9
$PEO_{20}LiTFSI$ with TTE	8.7

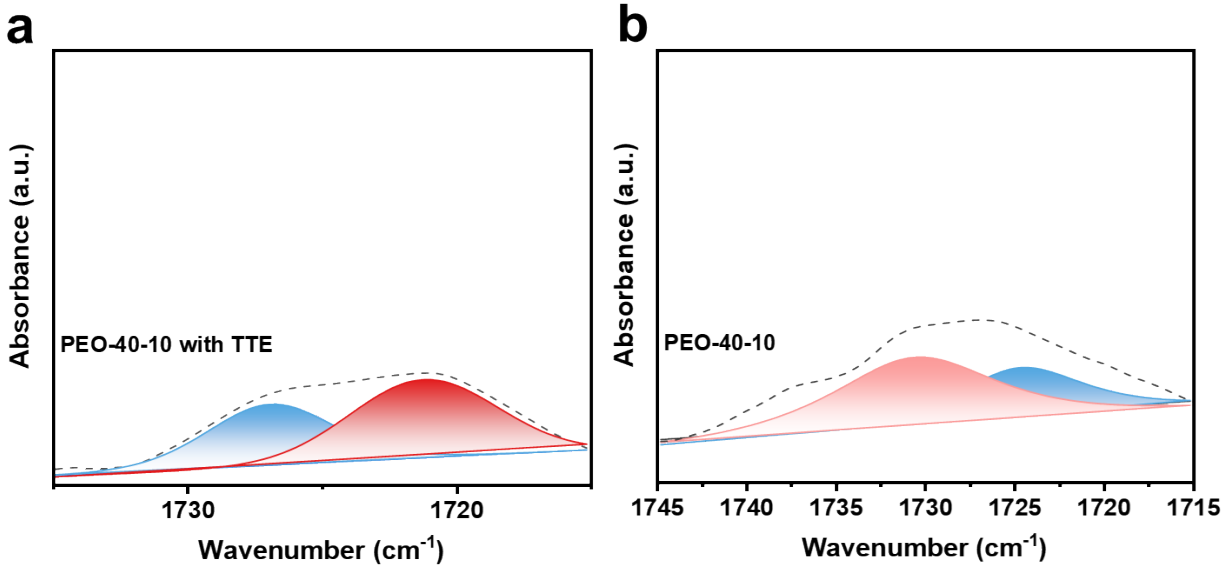

Figure S8 The peak-differentiating and fitting of FTIR. (a) PEO-40-10 with TTE (b) PEO-40-10

Table S11 The relative content of Li^+-coordinated C=O in PEO-40-10 with TTE and PEO-40-10

	Li^+-coordinated C=O	Free C=O
PEO-40-10 with TTE	57.7%	42.3%
PEO-40-10	35.9%	64.1%

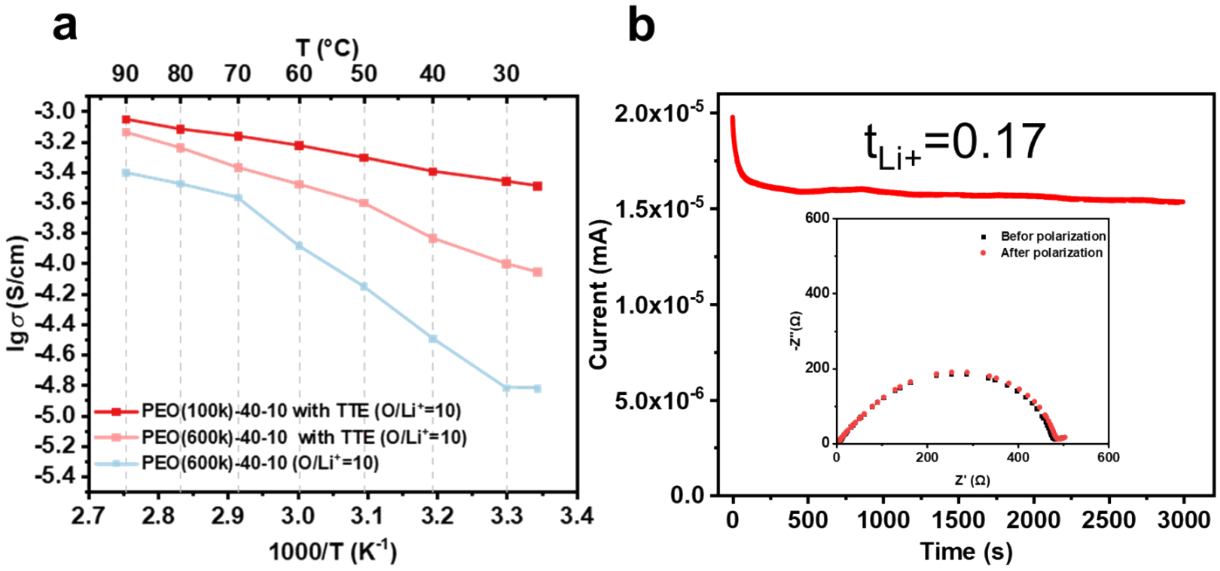

Figure S9 (a) The Arrhenius plot of PEO(100k)-40-10 with TTE (O/Li^+=10), PEO(600k)-40-10 with TTE (O/Li^+=10) and PEO(600k)-40-10 (O/Li^+=10); (b) Chronoamperometry curves of the Li/Li cell with PEO(600k)-40-10 with TTE (O/Li^+=10)

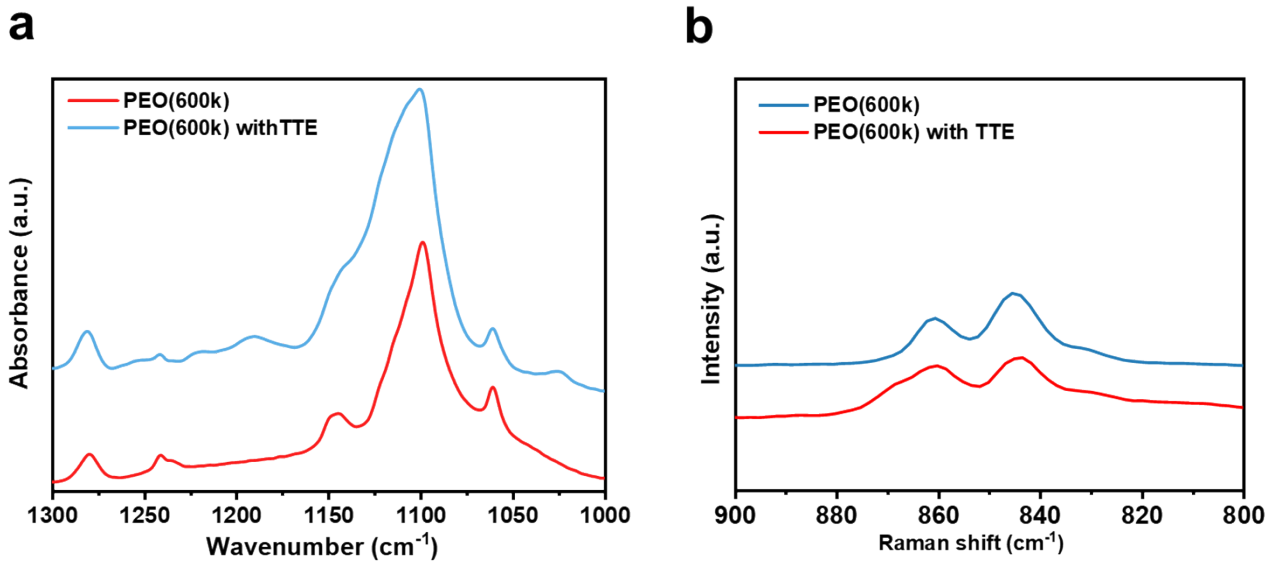

Figure S10 (a) The FTIR ranging from 1300 to 1000 cm^{-1} and (b) Raman spectrum ranging from 900 to 800 $cm^{-1}$of pure PEO(600k) with and without TTE.

Table S12 The simulated value of ionic conductivity of PEO_{20}LiTFSI and PEO_{20}LiTFSI with TTE at 80 ℃

	Ionic conductivity mS/cm
PEO_{20}LiTFSI with TTE	1.41
PEO_{20}LiTFSI	0.70

Table S13 The equilibrium swelling rate of PEO(600k) with TTE at 25 ℃

	$\frac{W\ (Swelling)\ -\ W\ (Dry)}{W\ (Dry)} \times 100\%$
PEO(600k) with TTE	2.24

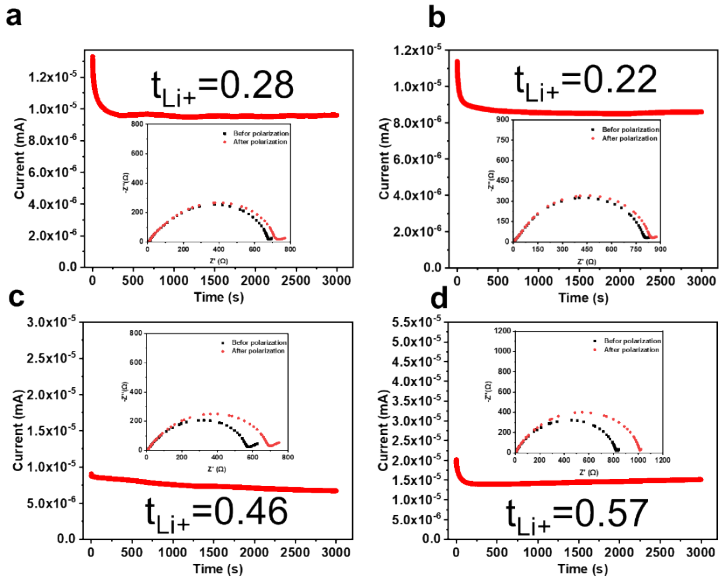

Figure S11 The chronoamperometry curves of the Li/Li cell for t_{Li+} (a) PEO-12 with TTE (b) PEO-10 with TTE (c) PEO-40-10 (SPE2900) with TTE (d) PEO-40-10 (SPE1100) with TTE

Table S14 The corresponding data to t_{Li+}

	R_0	R_{ss}	I_0	I_{ss}
PEO(600k)-40-10 with TTE	834.2	1,006.5	1.98E-05	1.52E-05
PEO-12 with TTE	669.7	726.6	1.32E-05	9.60E-06
PEO-10 with TTE	812.8	848.6	1.13E-05	8.60E-06
PEO-40-10 (SPE2900) with TTE	694.3	565.8	8.97E-06	6.71E-06
PEO-40-10 (SPE1100) with TTE	486.3	489.6	1.93E-05	1.50E-05

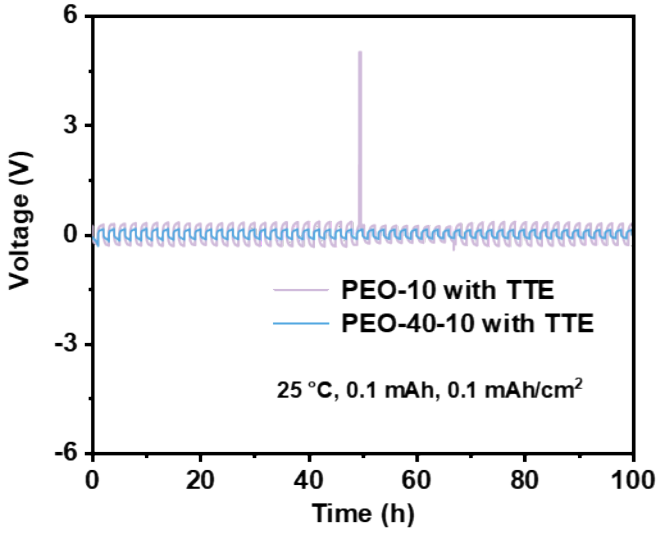

Figure S12 Plating/stripping performance of Li/Li cell based on PEO-10 with TTE and PEO-40-10 with TTE.

References

1. M. J. Abraham, T. Murtola, R. Schulz, S. Páll, J. C. Smith, B. Hess and E. Lindahl, *SoftwareX*, 2015, **1-2**, 19-25.
2. W. Humphrey, A. Dalke and K. Schulten, *J. Mol. Graphics*, 1996, **14**, 33-38, 27-38.
3. W. L. Jorgensen, D. S. Maxwell and J. TiradoRives, *J. Am. Chem. Soc.*, 1996, **118**, 11225-11236.
4. P. M. Anderson and M. R. Wilson *, *Mol. Phys.*, 2005, **103**, 89-97.
5. K. Shimizu, D. Almantariotis, M. F. C. Gomes, A. A. H. Padua and J. N. C. Lopes, *J. Phys. Chem. B*, 2010, **114**, 3592-3600.
6. S. Saito, H. Watanabe, K. Ueno, T. Mandai, S. Seki, S. Tsuzuki, Y. Kameda, K. Dokko, M. Watanabe and Y. Umebayashi, *J. Phys. Chem. B*, 2016, **120**, 3378-3387.
7. H. Hua, B. Huang, X. Yang, J. Cheng, P. Zhang and J. Zhao, *Physical Chemistry Chemical Physics*, 2023, **25**, 29894-29904.
8. H. Hua, X. Yang, P. Zhang and J. Zhao, *The Journal of Physical Chemistry C*, 2023, **127**, 17324-17334.
9. C. Calero, J. Faraudo and M. Aguilella-Arzo, *Mol. Simul.*, 2011, **37**, 123-134.